Journal of Catalysis **191,** 30–45 (2000)
doi:10.1006/jcat.1999.2765, available online at http://www.idealibrary.com on IDEAL®

A Study of Ethanol Reactions over Pt/CeO_2 by Temperature-Programmed Desorption and *in Situ* FT-IR Spectroscopy: Evidence of Benzene Formation

Anna Yee, Scott J. Morrison, and Hicham Idriss[1]

Materials Chemistry, Department of Chemistry, The University of Auckland, Private Bag 92019, Auckland, New Zealand

Received July 5, 1999; revised November 16, 1999; accepted November 19, 1999

The reaction of ethanol over unreduced and H_2-reduced 1 wt% Pt/CeO_2 has been investigated primarily by temperature-programmed desorption (TPD) and *in situ* Fourier transform infrared spectroscopy (FT-IR). Steady state reactions have been conducted to provide information regarding the kinetics of the above reaction. Characterisation of the catalyst has been achieved through the use of XPS and titration of surface metal sites with CO. XPS studies have shown that the addition of Pt partially reduces the CeO_2 surface, as indicated by the decrease in the O/Ce ratio from the stoichiometric value to 1.59. FT-IR studies have shown that ethanol adsorbs dissociatively to form two types of ethoxides (monodentate and bidentate). The presence of Pt resulted in a $\Delta\nu$(C–O) = ca. -20 cm^{-1}, for both species, with respect to observed ethoxide band positions on CeO_2 alone. This shift may indicate that these species are perturbed due to the presence of Pt^{2+} clusters and the surface oxygen vacancies associated with them. The oxidative dehydrogenation of these ethoxide species produces acetaldehyde on both the unreduced and H_2-reduced Pt/CeO_2 surfaces. Adsorbed crotonaldehyde species were observed and characterised by bands at 1657 and 1632 cm^{-1} corresponding to ν(C=O) and ν(C=C), respectively. TPD experiments have shown that between unreacted ethanol and acetaldehyde, benzene is produced in appreciable amounts from both the unreduced and H_2-reduced surfaces of Pt/CeO_2. The formation of benzene has been postulated to proceed via reaction of surface-bound crotonaldehyde and acetaldehyde species. Additional studies involving the adsorption of CO over H_2-reduced CeO_2 and Pt/CeO_2 have been conducted. FT-IR results show that CO does not adsorb appreciably on CeO_2. In addition to linear and bridged CO species, a tilted CO species was identified, by a broad band at ca. 1704 cm^{-1}, on Pt/CeO_2 following adsorption of CO. Carbonite species (1325, 1297, 1190, and 1082 cm^{-1}) were also detected on Pt/CeO_2 following adsorption of CO and subsequent heating. TPD following CO adsorption on both CeO_2 and Pt/CeO_2 have shown that the predominant desorption product is CO_2. CO_2 desorbs from both CeO_2 and Pt/CeO_2 in three temperature domains. The lower desorption temperatures, 400 and 525 K, correspond to oxidation of CO to CO_2 and decomposition of formate species, respectively. The high-temperature (700 K, CeO_2 and 578 K, Pt/CeO_2) CO_2 desorptions arise from the decomposition of hydrogenocarbonates and carbonate species.

INTRODUCTION

The interest of this study was largely motivated by the use of ceria (CeO_2) in automobile exhaust catalysts (three-way catalysts, TWC) and the environmental and health concerns associated with the use of oxygenated fuel components with such systems. The improved performance and efficiency of exhaust systems is fundamental in reducing the high levels of toxic pollutants emitted into the atmosphere. Since their introduction in the mid-1970s, catalytic converters have been instrumental in controlling automotive exhaust emissions by simultaneously oxidising CO and hydrocarbons and reducing NO_x.

Furthermore, increasing environmental and health concerns arising from high levels of automobile exhaust emissions has prompted many industrialised countries to introduce legislation mandating reductions in toxic emissions. As a consequence, oxygenated compounds, such as alcohols and ethers, are increasingly being used as fuel additives and, in the case of alcohols, also as alternative sources of fuel. Although alcohols are considered to be clean burning fuels, their partial oxidation to aldehydes poses a greater threat as potential carcinogens. The problem of effectively controlling the emissions caused by burning these oxygenated compounds requires a better understanding of the reaction pathways along which the desired conversions occur on current commercial catalyst systems. This greater understanding will thus facilitate the development of more suitable catalyst materials.

Hydrogen reduction of CeO_2 has been reported to begin at 473 K and to be a surface process, with temperatures above 923 K required for bulk reduction (1). Following treatment at high temperature in an oxygen-containing atmosphere, the oxidation of the metal in M/CeO_2 is promoted by ceria to a M–O complex. Such species have been

[1] Corresponding author: E-mail: h.idriss@auckland.ac.nz. Fax: +64 9 3737422.

0021-9517/00 $35.00

detected at ca. 700 cm^{-1} on Pt/CeO_2 with the use of Raman spectroscopy (2). The formation of *M*–O complexes have also been identified spectroscopically from other noble metals, demonstrating that the formation of an oxidised metal M^+/CeO_2 is a rather general phenomenon. Supporting noble metals on ceria or CeO_2-containing materials dramatically changes their redox behaviour. The addition of a few percent of a noble metal is reported to effectively promote the reduction of surface oxygen only (1, 3). Evidence of this effect has also been observed in XPS studies conducted within this laboratory (4): the addition of noble metals to the CeO_2 was found to effectively decrease the atomic oxygen-to-cerium ratio, thus indicating a reduction of the CeO_2 surface.

Alcohols have been found to adsorb to various metal oxide surfaces by heterolytic dissociation of the O–H bond, with the proton going to a surface lattice oxygen and the remaining alkoxide fragment adsorbed to the surface cation. For example, adsorbed methoxide species have been spectroscopically detected upon adsorption of methanol on various oxide surfaces, including CeO_2 (5–7), ZnO (8), Al_2O_3 (9) and MgO (10). The decomposition of alcohols over metal oxides can occur via dehydration (to alkenes), dehydrogenation (to aldehydes or ketones), or oxidation (to carboxylates) reactions. In some instances, coupling and bimolecular hydrogenation reactions can occur to produce higher hydrocarbons. The main body of literature on alcohol reactions over CeO_2-containing catalysts consists of predominantly of methanol oxidation. Spectroscopic studies by various authors have identified three methoxide species (monodentate, bidentate, and tridentate) from the adsorption of methanol on CeO_2 (5, 6, 11, 12). Similarly, previous work involving the reaction of ethanol over CeO_2 and Pd/CeO_2 showed that ethanol adsorbed via dissociation of the O–H bond to form ethoxide species (13).

Dehydrogenation of primary alcohols to aldehydes has been widely observed on various oxide surfaces. Subsequently, the oxidation of these aldehydes may result in the formation of carboxylate species if the surface contains oxygen of sufficient mobility. Other reaction pathways have also been observed on oxide surfaces from C_2 oxygenates, such as the following:

(1) Carbon–carbon bond formation from aldehydes is possible through aldolisation reactions. In particular, the β-aldolisation of two acetaldehyde molecules, with subsequent dehydration, produces crotonaldehyde. Such a reaction on a surface would require Lewis acid and base sites to bind the two molecules and abstract an α-hydrogen. Crotonaldehyde formation has been observed on the surfaces of CeO_2 (14), TiO_2 (15), Al_2O_3 (16), and β-UO_3 (16) among other surfaces, upon the adsorption of acetaldehyde.

(2) Abstraction of a hydrogen atom from acetaldehyde can yield an acetyl species, $CH_3C{=}O_{(ads)}$; (ads): adsorbed. Acetyl species have previously been observed from ethanol on Pd(111) (17) and from acetaldehyde on Pd(110) (18), Pd/CeO_2 (14), and Pt–Na/SiO_2 (19). Further reaction of an acetyl with an adsorbed methyl group can result in the production of acetone (14).

(3) Two adsorbed aldehyde molecules may donate their oxygen to a reduced surface and couple together, forming a symmetric olefin molecule. This reaction has been observed on reduced oxides, such as UO_2 (20), H_2-reduced TiO_2 (21), Fe_3O_4 (21), and CeO_2 (14).

The bonding of CO to surfaces has been frequently explained by the Blyholder model (22), which essentially utilises the frontier orbital theory in that only the HOMO and LUMO of the molecule, namely, the 5σ and 2π orbitals, are involved in the bonding. The bonding is considered to be derived from contributions arising from back-donation of electronic charge from the metal into the CO $2\pi^*$ orbital in conjunction with the donation of electronic charge from the CO 5σ orbital to the metal. Carbon monoxide is used commonly as a probe molecule in the study of the surface chemistry of both metals and metal oxides, via adsorption. This is evidenced by the numerous IR studies involving CO adsorption on various supported and unsupported oxides, including CeO_2 (23–26), Pt/CeO_2 (27), Pt/TiO_2 (28), Pd/CeO_2 (29–31), and Pd/SiO_2 (32). The adsorption of CO on noble metals is much stronger than that on oxides

Structure-sensitivity effects of the mode of CO absorptions over transition metals has received considerable attention. For example, it has been found that molecules at step sites exhibit different wavenumbers from those on terrace sites; however, the direction of the shift is dependent on the nature of the surface. π-Bonding, involving partially filled metal *d* orbitals, occurs between the metal atom and its surrounding metal atoms. CO molecules will consequently compete for *d* electrons of the central metal atom. Substituents that are not involved in π-bonding with the central metal atom afford stronger π-bonding between the metal atom and CO. Subsequently, the bond order of the C–O bond, together with the ν(CO) frequency, decreases as the π-character of the M–C bond increases.

Previous work involving the reaction of ethanol over CeO_2 and Pd/CeO_2 (13) has shown considerable differences in reaction products and pathways with respect to the addition of Pd to CeO_2. Consequently, the present work is devoted to understanding the reaction pathways of ethanol over Pt/CeO_2, with attention to discerning any effects due to the presence of Pt. The surface and the area near the surface were studied by XPS, CO titration, and BET. The reactions were followed by TPD and in steady state conditions while the surface adsorbates were monitored by *in situ* FT- IR. Parallel work related to CO adsorption modes over CeO_2 and H_2-reduced Pt/CeO_2 surfaces is also presented and discussed.

EXPERIMENTAL

Catalyst preparation and characterisation. Pt/CeO_2 (1 wt%) was prepared from an aqueous slurry of $PtCl_4$ (in 1 M HCl) with CeO_2 (preparation described elsewhere (13)) which was heated (383 K), with constant stirring, until the formation of paste and then dried at 373 K. Upon drying, the catalyst was calcined at 673 K for 3 h. Specific surface area measurements were determined by the multipoint BET method (33). Surface compositions were analysed by X-ray photoelectron spectroscopy (XPS); experimental details for the XPS setup were described in a previous work (13).

The chromatographic or "pulse-flow" technique was employed for particle size determination. The catalyst was contained in a glass fixed-bed reactor cell. The outflow of the reactor was connected to a three-way valve capable of diverting the gas flow either to the TCD or out to a waste stream. The catalysts investigated in this study were reduced under hydrogen flow at 523 K overnight and then cooled to room temperature under hydrogen flow. The system was then purged with helium for 15 min and the gas flow from the reactor diverted to the TCD. Carbon monoxide was introduced into a 0.25-ml sample loop and a pulse of CO was admitted into the reactor; additional 0.25-ml injections of CO were made until no further adsorption by the catalyst was detected.

Steady state reactions. Kinetic analysis was conducted with a fixed-bed reactor fitted in a programmable oven, with an operating range of up to 673 K and linked to a gas chromatograph (GC) via a six-way valve (containing a 1-ml loop). Ethanol, in a saturator at 273 K, was introduced via either a continuous flow of dry air, a mixture of dry air and helium, or helium only, depending on the experimental conditions. The GC was equipped with a flame ionisation detector (FID) and coupled to a PC running PEAKSIMPLE III software for data acquisition. A Chromosorb 102 column ($l = 2$ m, $d = 0.318$ cm), with nitrogen as the carrier gas, was used for the separation of organic compounds at 373 K. The gas, containing ethanol, was allowed to flow over the catalysts for 10 min at room temperature before samples were injected into the GC via the six-way valve. For Arrhenius plots, ethanol conversion was kept below 10%.

Fourier transform infrared (FT-IR) spectroscopy. IR spectra were recorded using a Digilab FTS-60 Fourier transform spectrometer at a resolution of 4 cm^{-1} and 100 scans/spectrum. Adsorption experiments were carried out in a stainless steel IR cell equipped with removable CaF_2 windows; the construction of this cell was described elsewhere (34). The catalyst sample was pressed into a self-supporting disc, ca. 15 mm in diameter. The cell was connected to a conventional vacuum line maintained at a base pressure of 5×10^{-5} Torr (1 Torr = 133.3 N m^{-2}) with a diffusion pump. Because of its basic nature, CeO_2 binds carbonates readily and to obtain a clean surface, pretreatment temperatures greater than 1000 K are often required. In this study, a temperature of 755 K was found to be sufficient. Pretreatment of the CeO_2-supported catalysts involved heating the sample at 755 K under oxygen (1.50 Torr) for 30 min followed by evacuation (5×10^{-5} Torr) at 755 K for 5 min; this procedure was repeated once more.

Reduction of the catalysts was achieved by either heating under H_2 in batch conditions (for ethanol adsorption) or by H_2 flow at atmospheric pressure. In the case of the CO adsorption experiments, CeO_2 was reduced at 755 K with H_2 flow for 17 h and cooled to room temperature (under H_2 flow). Pt/CeO_2 was reduced (without pretreatment under O_2) under H_2 flow at 473 K for 14 h and then cooled to room temperature under H_2 flow.

A typical IR adsorption experiment involved dosing ethanol (1.50 Torr), degassed by several freeze–pump–thaw cycles, or CO (3 Torr), onto the sample at room temperature for 3 min. A spectrum was taken upon evacuating the cell for ca. 15–25 min. The cell was then sequentially heated and spectra were collected, at room temperature (296–309 K), from 373 to 673 K in 50 K intervals. The spectra presented in this work are obtained by subtracting the spectrum of the catalyst sample prior to adsorption from that of the adsorbed sample. All spectra were recorded at room temperature.

Temperature-programmed desorption. Temperature-programmed desorption (TPD) experiments of the ethanol-adsorbed Pt/CeO_2 were undertaken following the methods described previously (13). TPD experiments of CO adsorbed catalysts were performed on 20- to 50-mg samples of H_2-reduced Pt/CeO_2 and CeO_2. The catalysts were contained in a 0.7-cm o.d. tubular quartz U-shaped reactor. Prior to adsorption, the catalysts were reduced under H_2 flow for 12 h at 523 K for Pt/CeO_2 and at 773 K for CeO_2. Upon reduction, the catalyst sample was cooled to room temperature under H_2 flow. Carbon monoxide was adsorbed on the reduced catalyst at room temperature for ca. 3 min. The outlet of the reactor was then connected to a pressure interface and the catalyst evacuated to ca. 10^{-2}–10^{-3} Torr for approximately 15 min to remove any reversibly adsorbed CO gas. The pressure interface was differentially pumped to ca. 10^{-3} Torr during operation by a two-stage rotary pump and was connected to the high-vacuum chamber (HVC) via a leak valve. The HVC was maintained at a base pressure of ca. 2×10^{-7} Torr. During TPD runs the pressure of the HVC was raised to 2×10^{-6} Torr by opening the leak valve to the reactor.

The catalyst temperature was raised, from room temperature, to 773 K at a rate of 15 K min^{-1}. The effluent from the reactor was analysed by a Leda-Mass quadrupole mass spectrometer that was coupled to a PC equipped with software (RGA for Windows) for acquisition of mass peak data. The mass spectrometer used in this study was

TABLE 1

Summary of Data Obtained from XPS, BET Surface Area Determination, and CO Titration of Surface Sites

	Pd($3d_{5/2}$)	Pt($4f_{7/2}$)	at.% Pd[a]	at.% Pt[a]	O/Ce[b]	$\Delta O/\%M$[c]	CO/M[d]	BET ($m^2\ g^{-1}$)
CeO_2 (13)	—	—	—	—	2.44[e]	—	0	57
1 wt% Pd/CeO_2 (13)	336.3 eV (PdO)	—	0.25	—	1.76	0.96	2	55
1 wt% Pt/CeO_2	—	74.0 eV (PtO)	—	0.26	1.59	1.58	3.5	63

Note. M: Pd, Pt. at.%: atomic percentage.

[a] Surface and near surface at.% as determined by XPS, for the as-prepared catalysts.

[b] XPS O(1*s*)/XPS Ce(3*d*)

[c] Is a measure of the degree of reduction of CeO_2 normalised per *M*. $\Delta O = 2 - x$, where x = O/Ce. The value of 2 is preferred because of stoichiometry.

[d] Irreversible CO adsorption at room temperature, 1 atm, over H_2-reduced surfaces. The amount of CO adsorbed was 0.23×10^{19} and 0.56×10^{19} molecules g^{-1} over Pd/CeO_2 and Pt/CeO_2, respectively.

[e] Excess O is due to contributions from surface hydroxyls and carbonates.

limited to monitoring 12 masses/cycle. To identify a product from mass spectral data, knowledge of the fragmentation pattern is required. Such patterns can be easily obtained by scanning the mass range of interest while leaking the desired gas into the vacuum system. However, lists of fragmentation patterns for numerous compounds are readily available. The relative yields of the desorption products were determined following the techniques used by other researchers (15, 35).

RESULTS

A. Characterisation and Steady State Kinetics

Table 1 presents the characteristics of 1 wt% Pt/CeO_2, together with previously characterised CeO_2 and Pd/CeO_2 (13) catalysts by BET, XPS, and CO adsorption at room temperature. Both metals are in an oxidised state in their as-prepared states. $\Delta O/\%M$ (as defined in Table 1) indicates that Pt has a higher reducing effect than Pd. Although the surface and near-surface atomic percent of both metals are very similar, CO adsorption clearly shows that Pt adsorbs more CO than Pd and that a 1 CO/1 *M* (M = Pd or Pt) ratio is most likely not a valid assumption for this system.

The reaction of ethanol has been conducted previously over CeO_2 and Pd/CeO_2 (13). The main reaction product was acetaldehyde, formed by oxidative dehydrogenation. Similar behaviour was observed for Pt/CeO_2 (this work). The reaction is first order with respect to ethanol and zero order with respect to oxygen. Table 2 presents the kinetic parameters of the reaction, including those of CeO_2 and Pd/CeO_2 for comparison. Pt/CeO_2 is less active than Pd/CeO_2 due to a slightly higher activation energy. Because of the relatively small activity of CeO_2 compared to that of *M*/CeO_2, the errors introduced for calculating the TON this way are negligible.

B. Adsorption of Ethanol on Unreduced 1 wt% Pt/CeO_2

(i) Temperature-Programmed Desorption

Figure 1 and Table 3 present the desorption profile and fractional yields, respectively, and show the existence of two distinct temperature domains. Acetaldehyde (*m*/*e* 29, 44, and 43) desorbs at the lowest temperature domain of 475 K with a shoulder at ca. 540 K. Ethanol (*m*/*e* 31, 45, and 29) desorbs also at 475 K but with a shoulder at ca. 600 K. Unreacted ethanol contributed to 45% of the total carbon desorbing. The highest temperature domain consists of several products. Methane (*m*/*e* 16 and 15) desorbs at 585 K with a carbon yield of 4.5% followed by CO_2 and CO, both at 610 K, representing 6 and 13%, respectively. Considerable amounts of benzene (*m*/*e* 78 and 77) are observed, also at 610 K, contributing by 24%. Benzene desorption from ethanol TPD over Pd/CeO_2 has been observed in a previous work, however, to a lesser extent (13). Acetone, previously observed over Pd/CeO_2 and CeO_2 during ethanol TPD, is absent (13). Crotonaldehyde, presumably formed by aldolisation of two molecules of acetaldehyde is observed in trace amounts at 520 K.

TABLE 2

Summary of Kinetic Data for the Reaction of Ethanol over CeO_2 and Pd/CeO_2 (13) and Pt/CeO_2 (This Work)

Catalyst	Activation energy, E_a ($kJ\ mol^{-1}$)	Pre-exponential factor, A ($ml\ g^{-1}\ s^{-1}$)	TON[a] at 400 K
CeO_2	75	4×10^9	—
Pd/CeO_2	40	5×10^5	8.6
Pt/CeO_2	43	6×10^5	2.6

[a] TON: number of ethanol molecules converted per atoms (Pt or Pd) per second. Atomic percent and BET surface areas required to calculate TON values are obtained from Table 1.

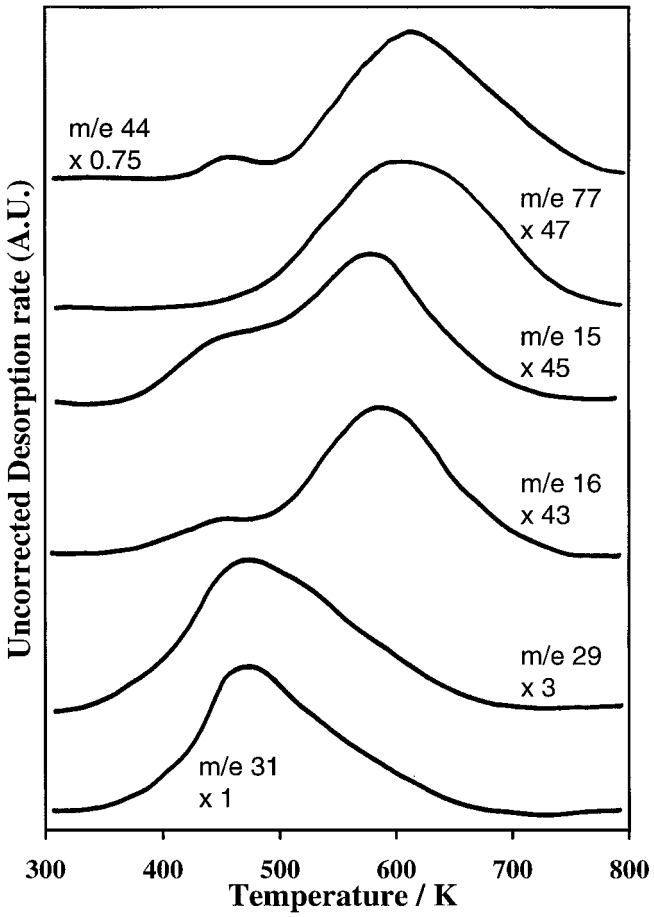

FIG. 1. Product desorption profiles from TPD after ethanol adsorption on unreduced 1 wt% Pt/CeO_2.

(ii) FT-IR after the Adsorption of Ethanol over Unreduced 1 wt% Pt/CeO_2

The adsorption of ethanol over Pt/CeO_2 at 309 K produced a spectrum with bands at 2977, 2633, 2910, 2878, 1902, 1480, 1450, 1399, 1352, 1339, 1264, 1080, and 1037 cm^{-1} attributed to multiple species (Fig. 2a). The formation of ethoxide species is evidenced by the bands at 2977 ($\nu_{as}(CH_3)$), 2933 ($\nu_{as}(CH_2)$), 2910 ($\nu_s(CH)$), 2878 ($\nu_s(CH_3)$), 1480 ($\delta(CH_2)$), 1450 ($\delta_{as}(CH_3)$), and 1399 cm^{-1} ($\delta_s(CH_3)$). Previous work over Pd/CeO_2 has shown the presence of two ethoxide species identified as mono- and bidentate species at 1078 and 1037 cm^{-1}, respectively (13). By analogy, the bands at 1080 and 1038 cm^{-1} are attributed to the (ν(C–O)) vibration of mono- and bidentate species, respectively (more details are given in the Discussion). Table 4 presents the types of alkoxide species and their corresponding ν(C–O) bands observed over CeO_2 and M/CeO_2. Ethoxides over both Pd/CeO_2 and Pt/CeO_2 surfaces have shifted to lower wavenumbers by ca. 20 cm^{-1} when compared to those observed over CeO_2 (a rationalisation of this behaviour is given in the Discussion).

The small band at 1902 cm^{-1} is attributed to bridged CO species. The band at 1264 cm^{-1} is assigned to $\tau(CH_2)$, although δ(OH) also gives a similar band. The negative band at 1601 cm^{-1} is due to water removal upon adsorption. This most likely results from dissociative adsorption of

TABLE 3

Product Analysis of Ethanol TPD over Unreduced 1 wt% Pt/CeO_2

Product	Peak temperature (K)	Yield	Carbon selectivity (%)
Ethanol	475	0.45	—
Acetaldehyde	475	0.035	6.4
Methane	585	0.045	8.2
Benzene	610	0.24	43.6
Crotonaldehyde	520	Traces	—
Acetone	—	0	0
CO	610	0.13	0.23
CO_2	610	0.06	10.9
Butene (m/e 56)	520	Traces	—

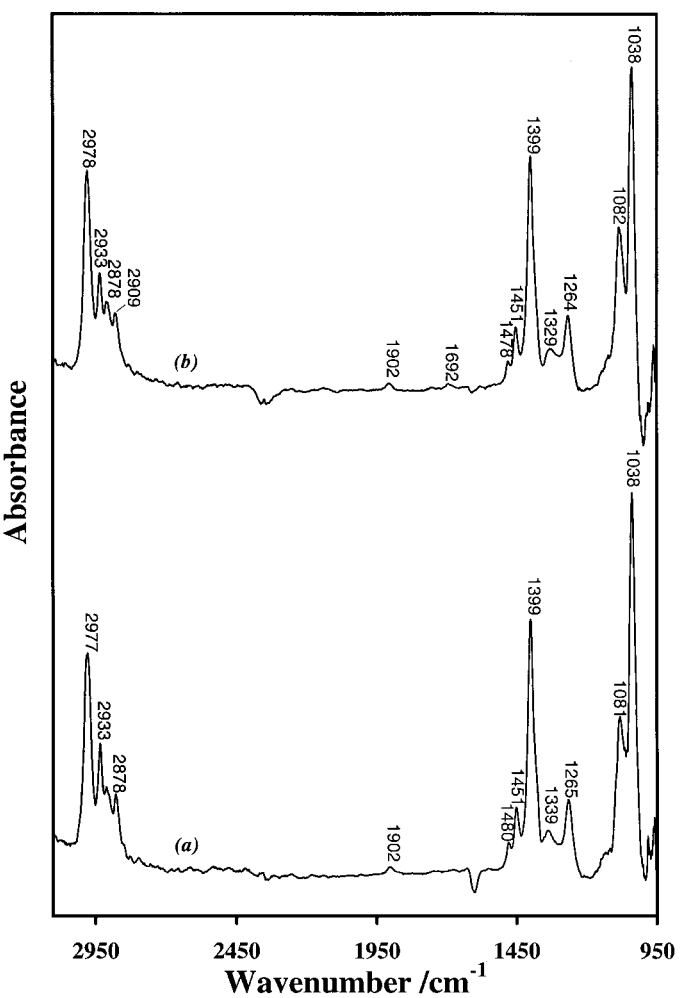

FIG. 2. IR spectra of (a) unreduced 1 wt% Pt/CeO_2 and (b) H_2-reduced 1 wt% Pt/CeO_2 following adsorption of ethanol at room temperature.

TABLE 4

Observed Wavenumbers for ν(C–O) Bands of Ethoxide and Methoxide Species on CeO_2

Assignment	Ethanol/ CeO_2 (13)	Methanol/ CeO_2 (5)	Methanol/ CeO_2 (6)	Ethanol/ Pd/CeO_2 (13)	Ethanol/ Pt/CeO_2 (this work)
ν(C–O)-t			1013	—	—
ν(C–O)-b	1057	1050	1057		
		1031		1037	1038
ν(C–O)-m	1107	1103	1104	1078	1080

Note. m, monodentate; b, bidentate; t, tridentate.

CH_3CH_2OH over surface OH, resulting in water formation that starts to outgas. It may also be due to displacement of irreversibly adsorbed H_2O by ethanol.

Heating to 373 K (Fig. 3a) caused small variations in the spectrum, while heating to 473 K (Fig. 3c) resulted in considerable changes. In addition to attenuation of ethoxide/ethanol peaks including the 1268-cm^{-1} band, four bands at 1352, 1545, 1580, and 1700 cm^{-1} are observed. The bands at 1352 and 1580 cm^{-1} are attributed to the symmetric and asymmetric stretches of ν(OCO) of a carboxylate species. The low wavenumber of the symmetric band suggests formate rather than acetate species (presumably formed via the CO recombination reaction with surface hydroxyls); it is also worth noting that the bridged CO band has decreased in intensity. CO adsorption over Pt/CeO_2 presented below (Fig. 11) also shows formate formation. A band at 1700 cm^{-1} is observed; ethanol adsorption over Pd/CeO_2 has also shown the presence of a similar band, which is attributed to adsorbed η^1-acetaldehyde (13). The production of acetaldehyde during ethanol TPD over both Pd/CeO_2 (13) and Pt/CeO_2 (this work) is an additional agreement to the attribution of the 1700 cm^{-1} band to η^1-adsorbed acetaldehyde (parallel IR spectra after adsorption of acetaldehyde over Pd/CeO_2 have also shown the presence of this band). This species is formed by the dehydrogenation of ethoxides.

Heating the catalyst to 523 K resulted in a further decrease of ethoxide species with a concomitant increase of the η^1-acetaldehyde band (1701 cm^{-1}). The bridged CO band at 1900 cm^{-1} disappeared and a weak band at 2128 cm^{-1} appeared. This latter band is due to weakly adsorbed linear CO over Pt^0. Both bands at 1354 and 1580 cm^{-1} (formate species) slightly increased in intensity. A band at 1534 cm^{-1} accompanied by another at 1387 cm^{-1} appeared. These bands are attributed to carbonate species. Other carbonates of oxide materials also gave these bands; these include α-Cr_2O_3 (1560/1340 cm^{-1}), La_2O_3 (1560/1340 cm^{-1}), Co_3O_4 (1545/1324 cm^{-1}), and $Na_6(Ce(CO_3)_5) \cdot 12\ H_2O$ (1560/1370 cm^{-1}) (36). Two distinct bands at 1657 and 1632 cm^{-1} are observed. We have previously studied these two bands (also observed over Pd/CeO_2) and attributed them to ν(C–O) and (ν(C=C) and $\rho(CH_3)$ of adsorbed crotonaldehyde species (13).

At 573 K, carbonate species increased and a 1430-cm^{-1} band also appeared. This latter band is attributed to a symmetric carbonate species. By 623 K mainly carbonate species are present on the surface (1628, 1529, 1429, and 1373 cm^{-1}). A small peak at 2122 cm^{-1} is still observed. The origin of this peak will be discussed latter.

C. Adsorption of Ethanol on H_2-Reduced 1 wt% Pt/CeO_2

(i) Temperature-Programmed Desorption

Carbon selectivity and fractional yields of reduced Pt/CeO_2 are shown in Table 5 while the desorption profiles

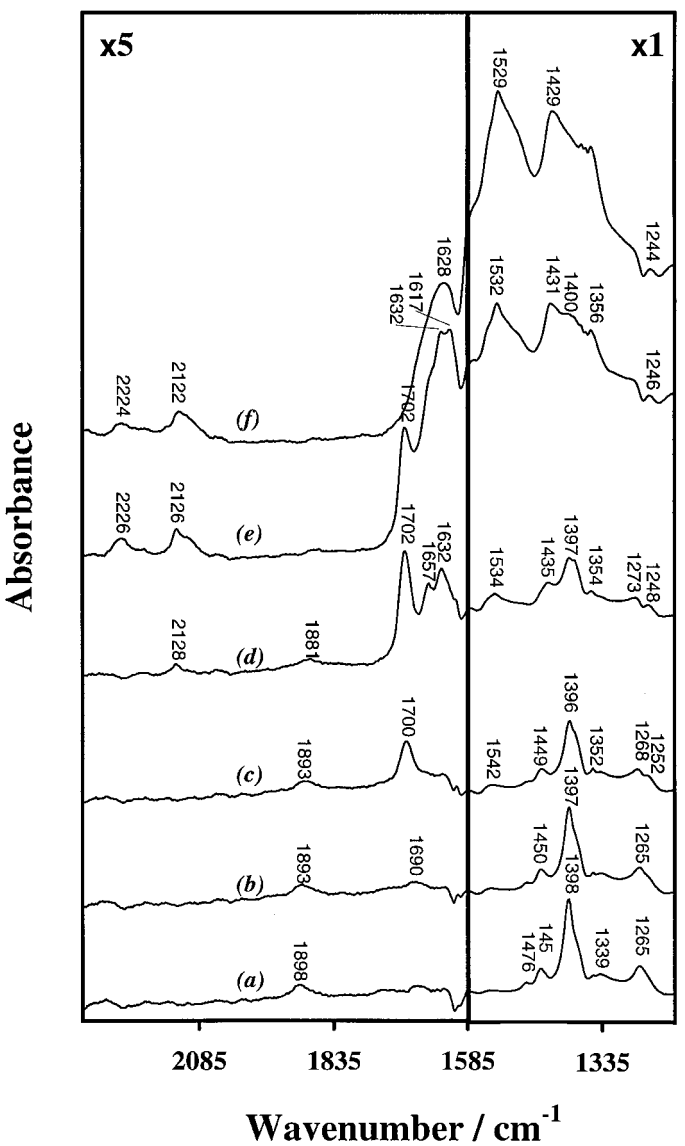

FIG. 3. IR spectra of unreduced 1 wt% Pt/CeO_2 following adsorption of ethanol at room temperature and heated to (a) 373 K, (b) 423 K, (c) 473 K, (d) 523 K, (e) 573 K, and (f) 623 K.

TABLE 5

Product Analysis of Ethanol TPD over H_2-Reduced Pt/CeO_2

Product	Peak temperature (K)	Yield	Carbon selectivity (%)
Ethanol	465	0.40	—
Acetaldehyde	465, 665	0.04, 0.065	6.8, 10.8
Methane	525, 665	0.22, 0.05	36.7, 8.8
Benzene	695	0.15	25.4
Crotonaldehyde	—	0	0
Acetone	695	0.001	0.2
CO	695	0.05	8.1
CO_2	695	0.02	3.5

are given in Fig. 4. The reduction of Pt/CeO_2 initiates different behaviour compared to that of the oxidised sample: (1) With the exception of the first acetaldehyde and ethanol desorptions, all products desorbed at higher temperatures. (2) Acetaldehyde desorbed in a distant peak in the high-temperature domain (665 K). (3) Benzene desorption shifted to 695 K and contributed to 15% of the carbon yield (about 60% of that observed on the unreduced surface). (4) Trace amounts of acetone (*m/e* 58, 43, and 15) were formed (695 K). (5) Crotonaldehyde desorption is not observed. (6) The reduced surface is slightly more active toward ethanol, evidenced by a decrease of the unreacted ethanol contribution to 40% while acetaldehyde desorption has increased 3-fold.

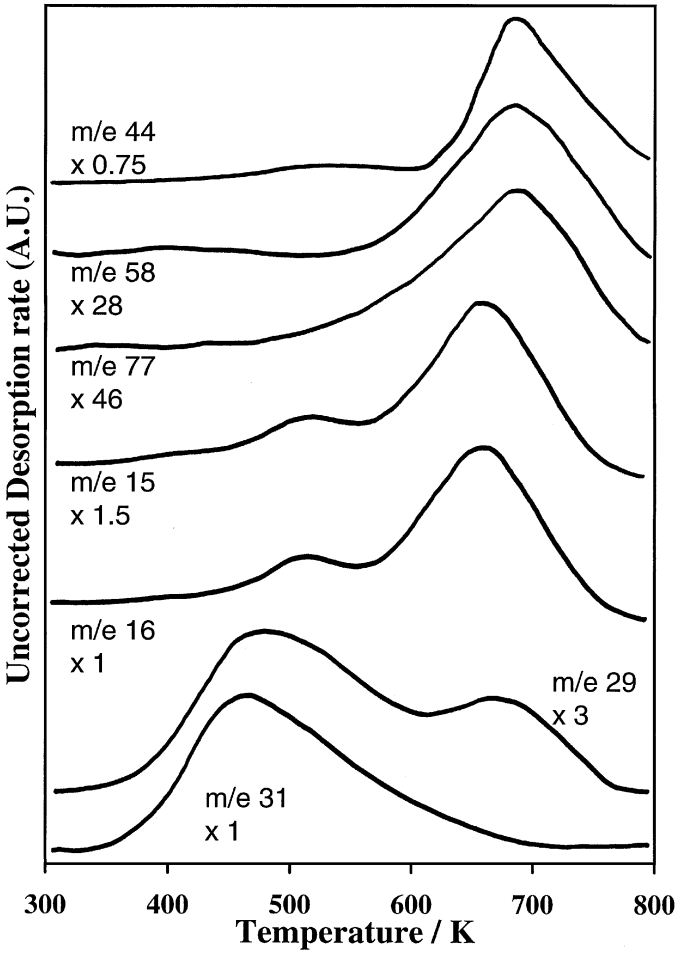

FIG. 4. Product desorption profiles from TPD after ethanol adsorption over H_2-reduced 1 wt% Pt/CeO_2.

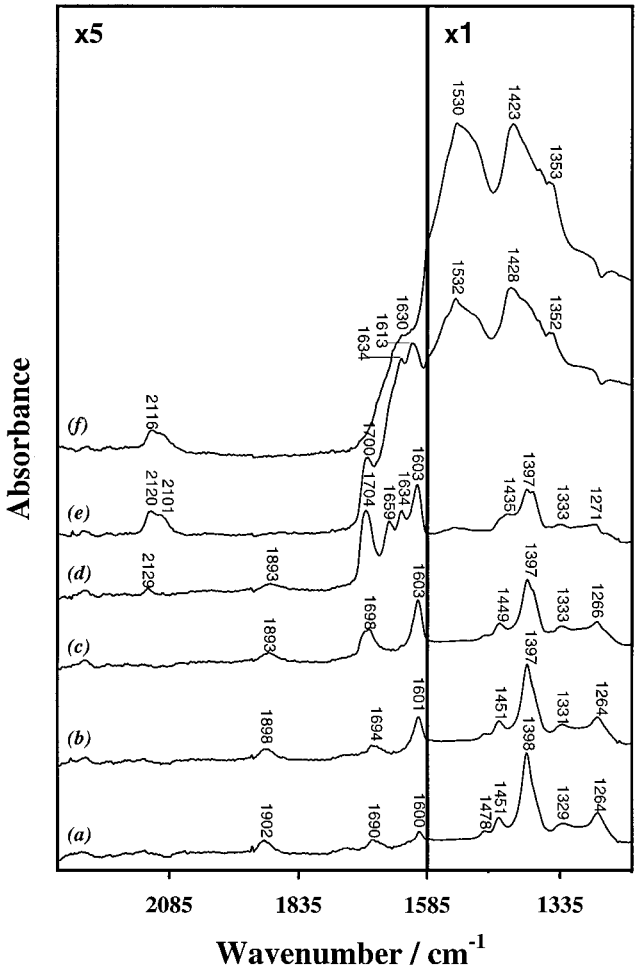

FIG. 5. IR spectra of H_2-reduced 1 wt% Pt/CeO_2 following adsorption of ethanol at room temperature and heated to (a) 373 K, (b) 423 K, (c) 473 K, (d) 523 K, (e) 573 K, and (f) 623 K.

(ii) FT-IR after the Adsorption of Ethanol over H_2-Reduced Pt/CeO_2

Figure 2b presents the absorption bands following ethanol adsorption over the H_2-reduced Pt/CeO_2 surface at 303 K. Very similar bands to those observed over the unreduced surface are also present on the reduced surface with two exceptions, however. The negative water peak is much smaller; this is expected since the majority of surface hydroxyls have been removed by H_2 reduction. A small peak at 1692 cm^{-1} is also present and is attributed to η^1-adsorbed acetaldehyde. Acetaldehyde formation was detected at 423 K (Fig. 5b) over the unreduced catalyst;

i.e., acetaldehyde is formed at ca. 100 K lower in this case. Heating the surface to 373 K (Fig. 5a) did not cause major changes. Acetaldehyde has increased slightly in intensity and a distinct 1600-cm^{-1} band (attributed to water) is observed. The latter may result from hydroxyl recombination with H atoms left on the surface upon reduction (hydroxyls, in this case, are formed from ethanol dissociation to ethoxides over O anions).

By 473 K (Fig. 5c), the acetaldehyde band (at 1698 cm^{-1}) has further increased in intensity. A band at 1144 cm^{-1} is clearly observed. This band is also characteristic of adsorbed acetaldehyde species (ν(C–O), ν(C–C)). A band at 1051 cm^{-1} is detected in the ν(C–O) region. At 523 K, IR bands attributed to ethoxide species have decreased in intensity. Evidence of the formation of crotonaldehyde species is given by the presence of two bands at 1634 and 1659 cm^{-1}. Carbonate species have also started to emerge (bands at 1536, 1435, and 1385 cm^{-1}); the acetaldehyde band was still intense (1703 cm^{-1}), however. Heating the surface to 573 K resulted in considerable formation of carbonate species (1532 and 1428 cm^{-1}) and total disappearance of the bridged CO species at 1890 cm^{-1}. In contrast, two bands at 2101 and 2120 cm^{-1} were clearly observed. At 623 K carbonates are the dominant species on the surface, although the two bands, 2101 and 2116 cm^{-1}, were still present.

Figure 6 presents the relative intensities of ethoxides, acetaldehyde, and carbonates IR bands as a function of reaction temperature for both unreduced and H_2-reduced surfaces. As expected, the formation of carbonate species start at higher temperatures on the reduced catalyst. The appearance of acetaldehyde on the reduced surface at lower temperatures indicates that the dehydrogenation of ethanol to acetaldehyde requires a lower activation energy than the unreduced one, although the relative abundance of acetaldehyde species on the unreduced surface is higher. Ethoxide behaviour is not considerably affected by the reduction.

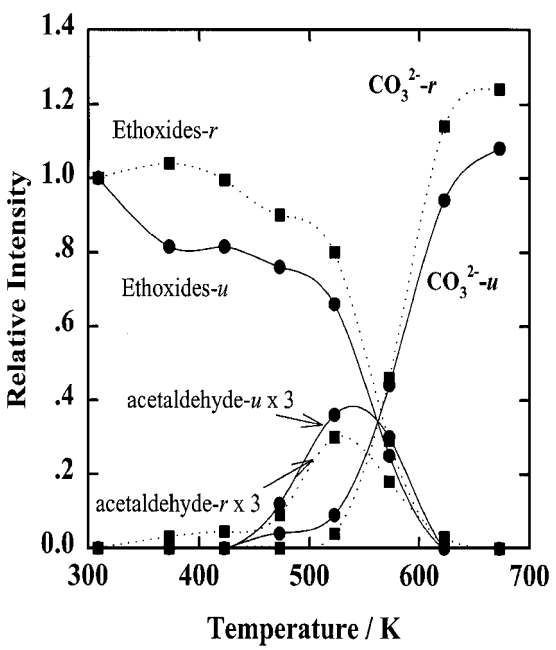

FIG. 6. Plot of relative intensity of ethoxide, acetaldehyde, and carbonate bands, from IR of ethanol adsorbed Pt/CeO_2, as a function of temperature: *u*, unreduced; *r*, H_2-reduced.

D. Adsorption of CO on H_2-Reduced CeO_2

(i) Temperature-Programmed Desorption

TPD experiments on H_2-reduced CeO_2 and H_2-reduced Pt/CeO_2 following CO adsorption were conducted to determine the existence, if any, of a relation between the desorption profiles of CO from TPD and the types of adsorbed CO (e.g., linear and/or bridged) and other adsorbates detected in IR studies. For instance, CO desorption from the Rh(111) and Rh(110) single-crystal surfaces exhibits desorption peaks at ca. 500 K and a shoulder at ca. 425 K (37, 38). The peak at 500 K was said to be due to the desorption of linearly bonded CO, while the shoulder at ca. 425 K was due to the desorption of bridge-bonded CO species. Furthermore, Diaz *et al.* (39) have reported that TPD following the adsorption of CO on H_2-reduced γ-Al_2O_3 produced a desorption peak at 170 K, which was assigned to the desorption of CO from Al^{3+} sites. Desorption peaks at 170 and 500 K were detected upon TPD of CO-dosed 5% Rh/Al_2O_3 and were assigned to CO desorption from Al^{3+} sites and the Rh overlayer, respectively.

TPD following the adsorption of CO at 296 K on prior H_2-reduced CeO_2 is presented in Fig. 7 and shows desorption profiles of m/e 44 (CO_2), 18 (H_2O), 2 (H_2), and 28 (CO). Other masses that were monitored but not observed included m/e 29 (–CHO, for aldehydes), m/e 15 (–CH_3, for alkanes), m/e 14 (–CH_2, for alkenes), m/e 31 (–CH_2OH^+, for alcohols), and m/e 27 (CH_2=CH–, for alkenes). m/e 16 was also observed but the absence of m/e 15 indicated that it is due to O fragments of m/e 44: CO_2. FT-IR studies have shown a band at 2121 cm^{-1} on the blank, H_2-reduced CeO_2 surface. This peak, which might be attributed to weakly adsorbed CO over Ce^{3+}, did not increase in intensity upon further CO adsorption at room temperature. However, it did decrease considerably upon heating at elevated temperatures to a third of its original intensity at 670 K. The weak desorption profile of CO observed in Fig. 7 may thus be in agreement with the decreasing intensity of the 2120-cm^{-1} band and its attribution to weakly adsorbed CO.

CO_2 was desorbed in three temperature domains: 400, 525, and 700 K. The first peak is in agreement with previously observed TPD of CeO_2, which was subjected to prior reaction with CO/H_2 at 488 K (1 atm) (40). This desorption indicates the capacity of CeO_2 alone to oxidise CO to CO_2, even at low temperatures. The second desorption at 525 K

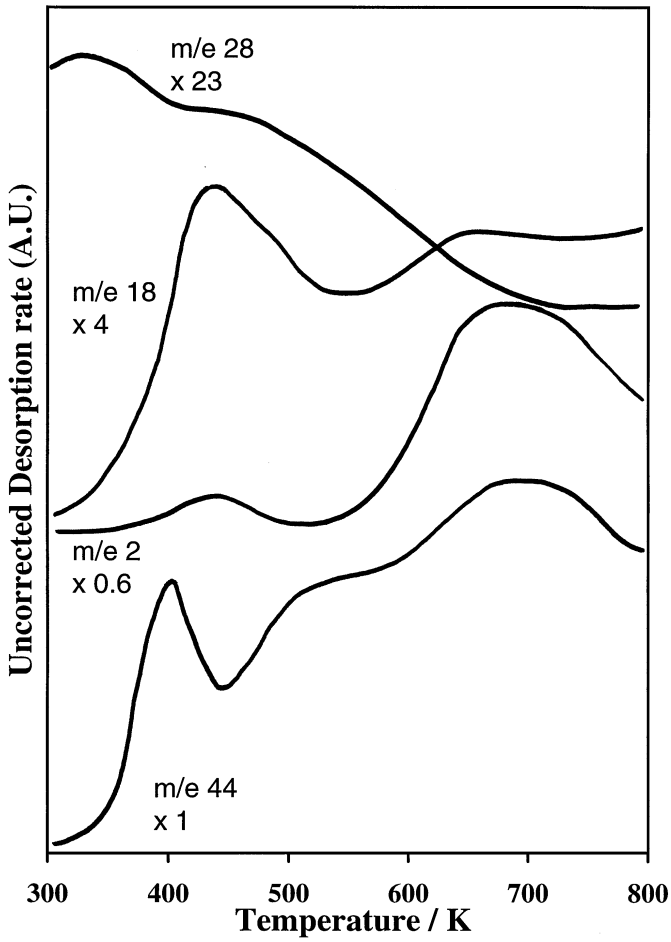

FIG. 7. Desorption profiles of selected masses from TPD of H_2-reuced CeO_2 following adsorption of CO at 296 K.

may be attributed to formate decomposition into CO_2 and CO. Formates are most likely formed through CO reaction with surface hydroxyls:

$$CO + OH_{(s)} \rightarrow HCOO_{(ads)}; \quad [1]$$

$$HCOO_{(ads)} \rightarrow CO_2 + \tfrac{1}{2}H_2 \text{ at } 525\,K. \quad [2]$$

The third desorption at 700 K also coincides with H_2 (m/e 2) desorption. This third CO_2 desorption at 700 K is most likely due to the decomposition of hydrogenocarbonates and carbonates.

The complementary nature of TPD and IR is well illustrated in Fig. 8, of which shows CO and H_2O desorptions during TPD superimposed over the negative IR bands at 2121 and 1611 cm^{-1}. The profile of the depletion of surface adsorbates, H_2O, and that of CO at 2121 cm^{-1}, matches perfectly with the TPD peaks of CO and H_2O. For example, by 550 K where no major changes in the water band intensity was observed (FT-IR), the major H_2O desorption (TPD) has occurred.

(ii) FT-IR Spectroscopy

The spectrum obtained after the exposure of CeO_2, with prior H_2 reduction at 770 K, to CO at room temperature (297 K, evacuated to 5×10^{-5} Torr) shows that CO does not adsorb appreciably on CeO_2 (Fig. 9). In effect, the undosed surface contains a peak at 2121 cm^{-1}. This peak might be attributed to irreversibly adsorbed CO species over Ce^{+3} cations (29). The latter is formed from the surface (as well as bulk) carbonate decomposition (reduction) during H_2 pretreatment. Other work has suggested that this peak may also be due to the $2F_{5/2} \rightarrow 2F_{7/2}$ transition of Ce^{+3} cations (7). This latter assignment will be discussed later. Thus, this observation suggests that adsorbed bridged CO species, observed in Figs. 2, 3, and 5, are adsorbed on the metal rather than on the oxide support. Heating the surface to 373 K accentuated the negative peak attributed to water at 1611 cm^{-1}. The negative features at ca. 2121 cm^{-1} may indicate loss of adsorbed CO. Weak bands at 1482, 1441, and 1348 cm^{-1} were detected (carbonates). The intensity of these bands increased with temperature, except for the band at 1482 cm^{-1} which was eliminated by 673 K.

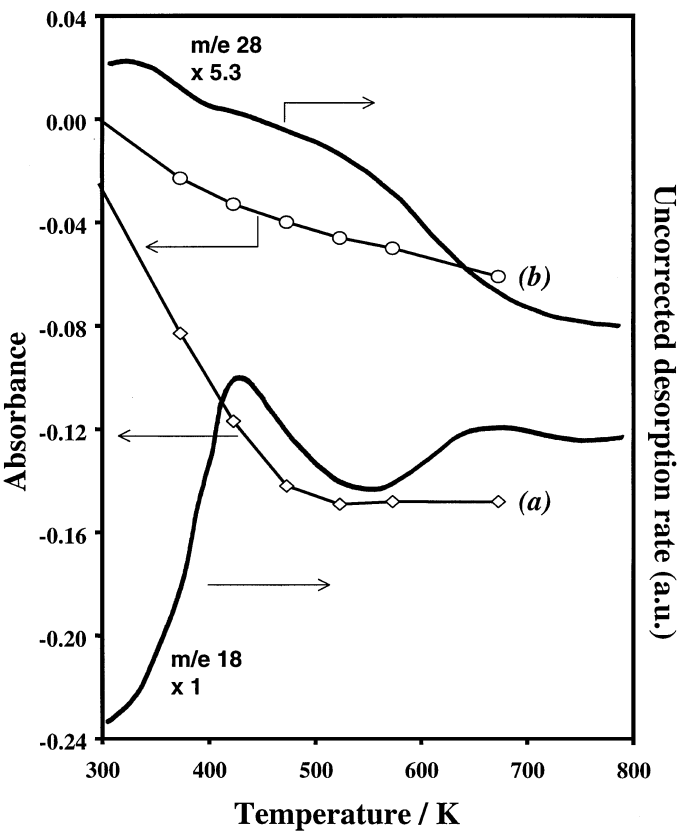

FIG. 8. Intensities of the negative bands detected at (a) 1611 cm^{-1} and (b) 2121 cm^{-1} corresponding to the loss of water and CO, respectively, superimposed against the desorption profiles for water (m/e 18) and CO (m/e 28) obtained from the TPD of H_2-reduced CeO_2 following adsorption of CO at 296 K.

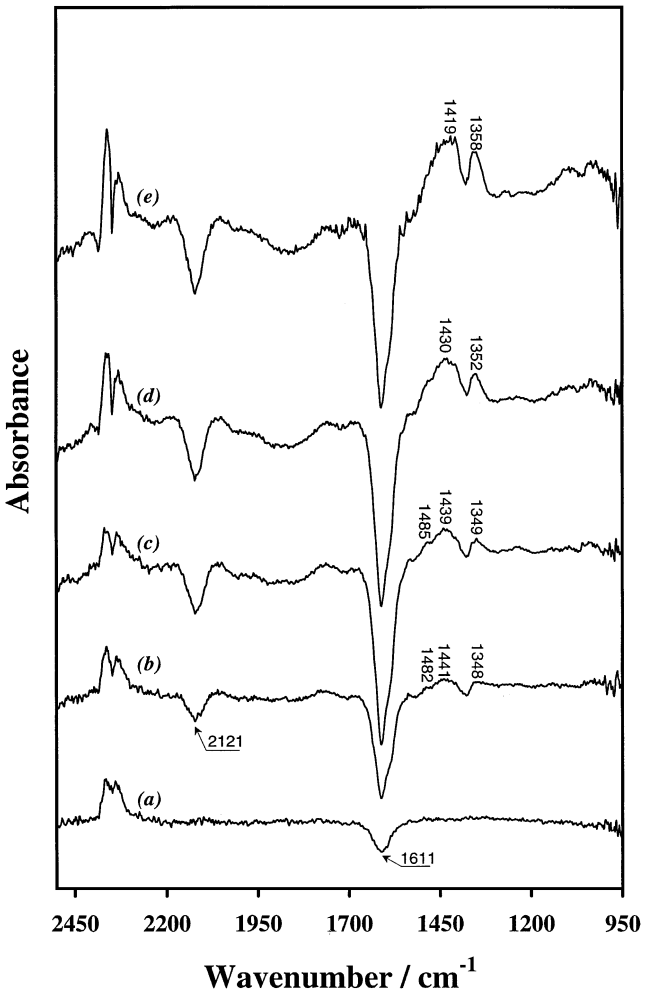

FIG. 9. IR spectra of H_2-reduced CeO_2 following adsorption of CO at (a) 297 K and heated, under vacuum, to (b) 373 K, (c) 473 K, (d) 573 K and (e) 673 K.

E. Adsorption of CO over H_2-Reduced 1 wt% Pt/CeO_2

(i) Temperature-Programmed Desorption

Figure 10 presents the desorption profiles for *m/e* 44 (CO_2), 18 (H_2O), 2 (H_2), and 28 (CO) obtained from TPD after the adsorption of CO at 296 K over Pt/CeO_2 previously reduced under H_2 at 523 K. The desorption profiles did not appear to differ significantly from those of CeO_2. CO_2 was again desorbed in three temperature domains: 400, 525, and 578 K. The first desorption peak at 400 K, occurring at the same temperature observed for the first CO_2 desorption on CeO_2, coincided with a weak H_2 desorption peak at the same temperature. However, the corrected amount, per unit area, of CO_2 desorbing is ca. 0.5 times smaller than that of CeO_2 alone. Formate species were detected in FT-IR spectra following the adsorption of CO on H_2-reduced Pt/CeO_2 at room temperature (Fig. 11a). However, these species were eliminated upon heating to 373 K. Thus, the CO_2 desorption at 400 K may be due to both formate decomposition and direct oxidation of CO to CO_2. A second CO_2 desorption occurred at 525 K, coinciding with the tail of the H_2 desorption peak at 400 K. This desorption, not very well resolved, may be due to formate species in a different environment, probably far from Pt sites. The third CO_2 desorption at 560–600 K, occurring with the desorption of H_2, arises from the decomposition of hydrogenocarbonate and carbonate species probably assisted by Pt.

(ii) FT-IR Spectroscopy

Figure 11a presents the spectrum obtained upon adsorption of CO on H_2-reduced Pt/CeO_2 at 295 K. Bands at 2068, 1844, 1765, 1704, 1561, 1370, and 1327 cm^{-1} were observed.

Bands attributed to adsorbed CO. The strong band at 2068 cm^{-1} is attributed to linearly adsorbed Pt^0–CO species and the band at 1844 cm^{-1} correlates well with 2-fold bridged CO species adsorbed on Pt(111) surfaces (41–43). The band at 1765 cm^{-1} is likely to denote the presence of 3-fold bridged CO species. A similar band at 1795 cm^{-1} was

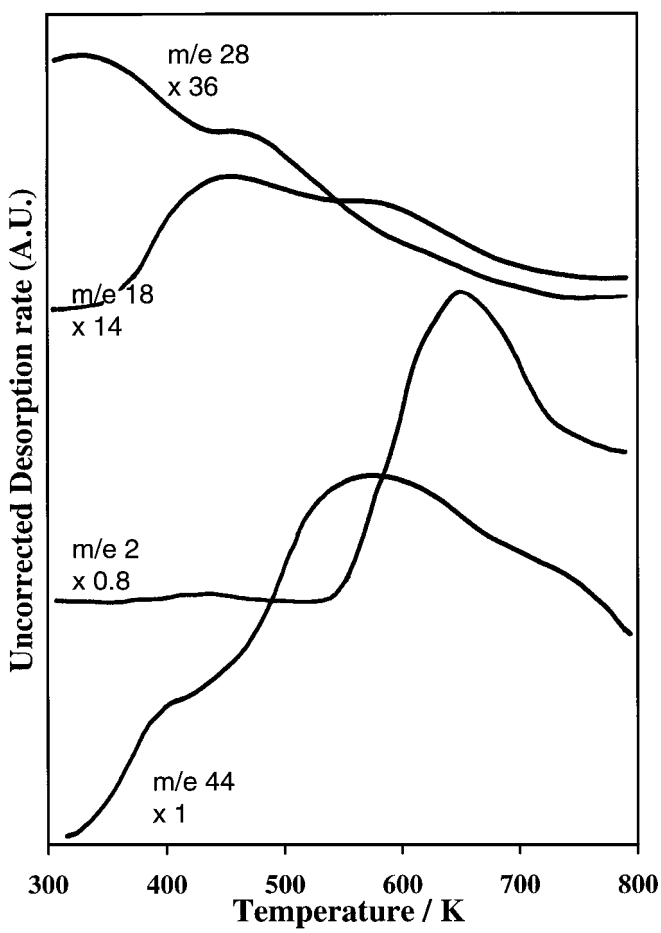

FIG. 10. Desorption profiles of selected masses from TPD of H_2-reduced Pt/CeO_2 following adsorption of CO at 296 K.

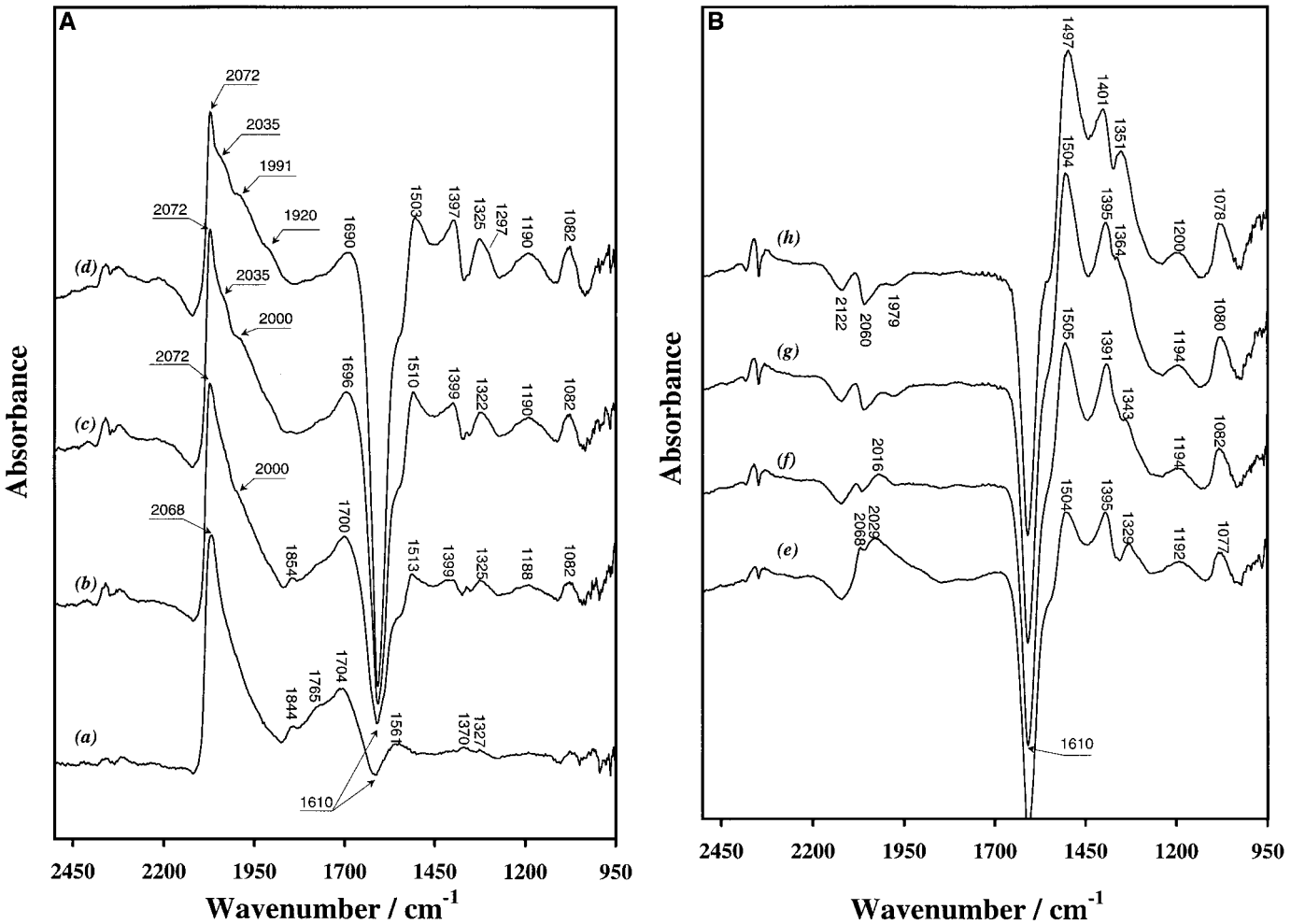

FIG. 11. (A) IR spectra of H_2-reduced Pt/CeO_2 following adsorption of CO at (a) 297 K and heated, under vacuum, to (b) 373 K, (c) 423 K, and (d) 473 K. (B) IR spectra of H_2-reduced Pt/CeO_2 following adsorption of CO at 297 K and heated, under vacuum, to (e) 523 K, (f) 573 K, (g) 623 K, and (h) 673 K.

reported by De la Cruz and Sheppard (44) from the adsorption of CO on Pt/SiO_2 at 300 K. The band at 1704 cm^{-1} is not related to an adsorbed formaldehyde species. TPD after CO adsorption (see above) shows the absence of formaldehyde desorption. Thus, it is most likely related to a tilted CO species, adsorbed through both the carbon and oxygen ends (19, 30). Upon heating the sample to 373 K (Fig. 11b), the band at 2068 cm^{-1} was shifted to 2072 cm^{-1} with a shoulder at ca. 2000 cm^{-1}. The spectrum obtained upon heating to 423 K shows an additional shoulder at 2035 cm^{-1}. A third shoulder was detected at ca. 1920 cm^{-1} following an increase in temperature to 473 K. A significant decrease in the intensity of the band envelope was observed upon heating to 523 K (Fig. 11e), with the band at 2072 cm^{-1} downshifted to 2068 cm^{-1} and the formation of a prominent peak at 2029 cm^{-1}. By 573 K the bands at 2068 and 2029 cm^{-1} were completely eliminated, with a weak band at 2016 cm^{-1} persisting. The bands corresponding to adsorbed CO disappeared by 623 K. The negative bands at 2122, 2060, 1979, and 1610 cm^{-1} (Fig. 11h) are due to residual species present on the H_2-reduced Pt/CeO_2 background spectrum.

Bands attributed to formate species. The weak bands at 1561 and 1370 cm^{-1}, observed at room temperature, are attributed to the asymmetric and symmetric OCO stretches of adsorbed formate species. The increased intensity of the negative water peak partially masks the asymmetric mode of formate. However, the symmetric band at 1370 cm^{-1} shows an increase at 373 K followed by a decrease at 423 K. By 473 K this band became very small.

Bands attributed to carbonite species, (CO_2^{2-}). Similar bands to those observed at 1325, 1297, 1190, and 1082 cm^{-1} (Fig. 11d) were reported by other workers upon CO adsorption on CeO_2 reduced under H_2 at 873 K (23). The authors

observed bands at 1300, 1270, 1160, and 1071 cm^{-1} and attributed them to two types of carbonite dianion (CO_2^{2-}) species (23). The bands at 1300 and 1160 cm^{-1} were assigned to carbonite species with C_{2v} geometry, whilst the bands at 1270 and 1071 cm^{-1} were attributed to species with C_s geometry. These assignments were made from a comparison with spectra of matrix isolated Cs_2CO_2 species. The bands observed at 1325, 1297, 1190, and 1082 cm^{-1} in this work agree well with those reported by Binet *et al.* (23) and hence are assigned to adsorbed carbonite species, with the bands at 1325 and 1190 cm^{-1} attributed accordingly to a carbonite species of C_{2v} geometry and those at 1397 and 1082 cm^{-1} to carbonite species of C_s geometry. At 573 K the bands at 1329, 1297, and 1082 cm^{-1} were removed, while the band at 1190 shifted to 1194 cm^{-1}. This latter band (which shifted to 1200 cm^{-1}) persisted even after heating to 673 K. Carbonates dominated the spectra at high temperatures.

DISCUSSION

A. Ethoxide and Carboxylate Formation

IR spectra have shown that ethanol adsorbs on the surfaces of Pt/CeO_2 via dissociation of the O–H bond to form adsorbed ethoxide species. The majority of reactions involving the adsorption of alcohols such as methanol and ethanol proceed via an alkoxide species intermediate formed from the scission of the O–H bond. Interestingly, the bond energy of the O–H bond (471.0 kJ mol^{-1}) is much greater than that of the C–O bond (338.7 kJ mol^{-1}) of an ethanol molecule (45). One would assume that the adsorption of ethanol would involve cleaving the C–O bond since it possesses the lowest bond energy to overcome. Yet the majority of surface studies involving the adsorption of alcohols have shown that dissociation of the O–H bond predominates to produce surface alkoxide species. A compilation of this work can be found in Ref. (46) where the authors clearly show that it is the O–H bond that first dissociates over (2 × 1) Pt (110) single-crystal surface. The reason for this behaviour is due to the phenomenon called the "proximity effect". Bonds tend to break when they are in relatively close proximity to the surface. The adsorption of alcohols on ionic surfaces, like CeO_2, is believed to involve dipole-induced dipole bonds, as shown below.

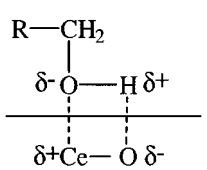

The dipole is strongest near the oxygen, and consequently the interaction with the surface is maximised if the oxygen of the alcohol is directed toward the surface. The formation of a metal–oxygen bond (*M*–O) is much easier from this configuration and thus O–H scission dominates.

Table 4 presents the band frequencies of the ν(C–O) of the ethoxides on Pt/CeO_2 from this work as well as those over CeO_2 and Pd/CeO_2 (13). The ν(C–O) bands are situated at 1057 and 1107 cm^{-1} on CeO_2 and in the presence of the noble metal (Pd or Pt) are shifted to ca. 1038 and 1080 cm^{-1}. To assign the species related to these bands, several points need consideration. First, we need to know to which element these alkoxides are bound since they can be bound to Pt or Ce cations. Alkoxide species have been detected on Pd(111) (44) and Pt(111)–$p(2 \times 2)$O (47); however, these species have only been stable at low temperatures, 200 and 170 K, respectively. This instability is due to the large negative enthalpies of adsorption which thermodynamically favour complete decomposition with a correspondingly low activation barrier. First, one thus may conclude, given the stability of ethoxides species observed in this work, that they are over Ce cations. Second, since the coordination number of Ce cations in CeO_2 depends on the surface structure, then a more detailed investigation of CeO_2 surfaces may help in assigning the mode of adsorption of these ethoxides.

Theoretical work investigating the surfaces of CeO_2 was conducted by other workers (48). The authors concluded that the (111), (110), and (310) will dominate the morphology of the material. On one hand, the (310) surface (which is a so-called type I surface; i.e., it is charge neutral with stoichiometric proportions of anions and cations in each plane, and the potential for each plane is exactly zero due to cancellation of the effects of the positive and negative charges and therefore has no dipole moment perpendicular to the surface) has *distinct step sites*. One can view these sites as active sites for dissociation as well as other reactions. On the other hand, the (111) surface of CeO_2 is a type II surface; i.e., the surface terminates with a single anion plane and consists of a neutral three-plane repeat unit and no dipole moment perpendicular to the surface (48). Although surface energy calculations of relaxed (111), (110), and (310) surfaces of CeO_2 are 1.95, 1.575, and 2.475 J m^{-2} respectively, the (310) is the most stable when surface oxygen vacancies are formed (48). This is the reason why it is the most active surface for the oxidation of CO to CO_2. Considerable amounts of CO_2 desorbed during CO TPD of CeO_2 may thus be interpreted as indication of the presence of exposed (310) surface planes.

Figure 12 shows a schematic representation of ethoxides over the CeO_2 (310), (111), and Pt/CeO_2 (111) surfaces. The (111) surface contains terminating O^{2-}, while Ce^{4+} cations are in the second layer and was recently observed by STM (49). It is highly unlikely that a nondefected (111) surface can accommodate ethoxides in a bidentate mode due to $O^{2-}_{(lattice)}$–$O_{(ethoxides)}$ electronic repulsion. However, it may accommodate ethoxides in a monodentate mode if the spacing between two surface oxygen anions is large enough to

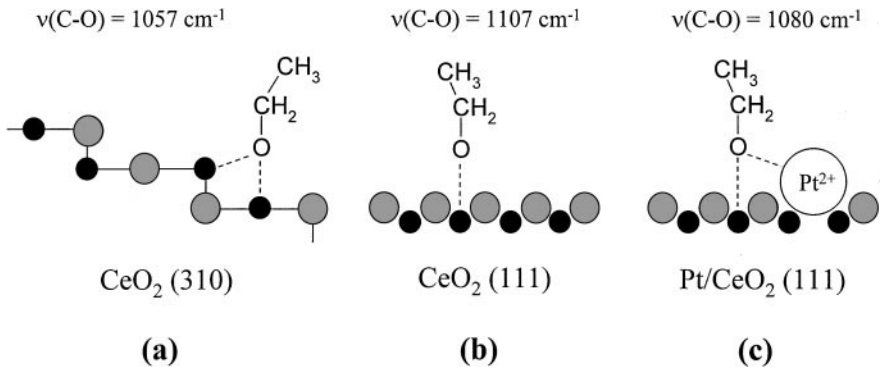

FIG. 12. Schematic depiction of ethoxide adsorption on the (a) CeO_2 (310), (b) CeO_2 (111), and (c) Pt/CeO_2 (111) surfaces. The grey circles represent the oxygen anions (ionic radius: 1.32 Å), the black circles represent the Ce^{4+} cations (0.92 Å), and the large unfilled circle labelled Pt^{2+} can be considered as a cluster of size, $n \approx 10$.

allow electronic interactions between $O_{(ethoxides)}$ and Ce^{4+} cations in the second layer. Such a mode of adsorption may be responsible for the 1107-cm^{-1} band observed on CeO_2. On the other hand, the (310) is a stepped surface containing two alternating Ce^{4+} cations in a step-flat configuration and two Ce^{4+} cations in a kink-flat configuration. An ethoxide may thus be formed over two step-flat Ce^{4+} cations, giving rise to bidentate species observed at 1057 cm^{-1}.

Next, we turn to the effect of metal addition on these two bands. Basically, both configurations are retained but at lower frequencies. Surface growth and segregation of Pt, Pd, and Rh over CeO_2 have been studied by several workers. A theoretical work by Sayle *et al.* (50) found that (in the case of Pt) Pt^{2+} are the most stable cations on the CeO_2 surface. This is in agreement with our XPS analysis showing lines corresponding to PtO (Table 1). The authors also found that Pt^{2+} segregate together with oxygen vacancies on the surface. This also is in agreement with the decrease of XPS O(1*s*)/Ce(3*d*) ratios in the presence of Pd (13) or Pt (this work) when compared to that of CeO_2 alone (Table 1). This latter finding results in modifying the adsorption and catalytic activity of CeO_2. An ethoxide adsorbed on a Ce cation that is close to an oxygen vacancy, as well as to a Pt cluster, will be bound to the surface in a stronger mode than another ethoxide species far from Pt. Indeed, the shift of the ethoxide bands to lower wavenumbers (over Ce cations in the presence of metal cations) is in accord with such a picture. Thus, the two distinct bands at 1080 and 1038 cm^{-1} are attributed to ν(C–O) of ethoxides at the interface between Pt (or Pd) and $Ce^{4+,3+}$–O^{2-}. The shoulder at 1059 cm^{-1} (in the case of Pt/CeO_2) is most likely due to bidentate ethoxides over $Ce^{4+,3+}$–O^{2-} centres far from the metal.

On the surface of bare unreduced CeO_2, ethoxides were readily oxidised into acetates; however, on M/CeO_2 (M = Pd (13) and Pt), acetate species are not observed. The absence of acetate formation is another consequence of the formation of surface oxygen anion vacancies. Basically, the partial reduction of the oxide support incurred by the addition of M (creation of oxygen vacancies) inhibit the oxidation pathways. The interesting observation is that H_2 reduction is not required to block this pathway. Moreover, ethanol-TPD data also shows that CO_2/CO ratios are decreased with increasing degree of reduction, $\Delta O/\%M$: CO_2/CO were 1.17 and 0.46 for Pd/CeO_2 (13) and Pt/CeO_2 (this work), respectively. $\Delta O/\%M$ were 0.96 and 1.58 for Pd/CeO_2 (13) and Pt/CeO_2 (this work), respectively.

B. Adsorption, Desorption, and Formation of CO

The bands at 2072 and 2035 cm^{-1} correspond to linearly bonded CO situated on reduced Pt^0 sites. The low-frequency bands at 2035 and 2016 cm^{-1} may indicate the presence of adsorbed sites of exceptional electron-donating power, such as on atomically rough parts of the surface or on isolated corner sites where dipolar coupling interactions are minimised because of the different directions of the CO vibrator relative to those situated on terrace sites (44). Such sites can strengthen the bonding between the CO and the metal surface and thus shift the ν(CO) band to lower frequencies. Indeed, other researchers investigating CO adsorption over Pd/CeO_2 observed similar bands. They assigned the 2072 cm^{-1} to O≡C–Pd^0 without Ce^{3+} interaction and the one at 2030 (2035 cm^{-1} for Pt/CeO_2 in this work) to O≡C–Pd^0 with Ce^{3+} interaction. Upon annealing to 423 K (Fig. 11c) a second shoulder is observed at 2000 cm^{-1}. This band is assigned to a compressed bridged CO (a similar band was observed over Pd/CeO_2 by other workers (29)). It is also worth indicating that both shoulders (2035 and 2000 cm^{-1}) become noticeable when the 1844 cm^{-1} (bridged CO) disappears (Fig. 11d).

Tilted CO Species

The broad bands at 1765 and 1700 cm^{-1} (Fig. 11A) are attributed to a tilted CO species, where both the C and O ends of the CO molecule are coordinated to the surface. Both bands were eliminated by 573 K, although the 1765-cm^{-1} band appeared to disappear first. Such species

TABLE 6

Band Positions of Adsorbed CO Species

IR band (cm^{-1})	Assignment (this work)	Similar bands (other works)
2068–2072	OC–Pt^0 (without Ce^{3+} interaction)	OC–Pd^0 (without Ce^{3+} interaction) (29) OC–Pt{100}–hex (56)
2035	OC–Pt^0 (with Ce^{3+} interaction)	OC–Pd^0 (with Ce^{3+} interaction) (29)
2000–1991	Compressed bridged CO on Pt^0	Compressed bridged CO on Pd (29)
1845	Bridged CO on Pt^0	Bridged CO on Pt{100}–hex (56) Bridged CO on Pt–Na/SiO_2 (19) Bridged CO on Ru(001) (57)
1765	Pt^0–CO–Ce^{3+}	Pd^0–CO–Ce^{3+} (30) Rh^0–CO–Nb^{x+} (58)
1700–1690	Pt_2^0–CO–Ce^{3+}	Pd_2^0–CO–Ce^{3+} (30) Rh_2^0–CO–Nb^{x+} (58)

were frequently observed by other workers. However, a brief treatment of the effect of surface structures on the mode of adsorption of CO is worth indicating before mentioning other works. Edge and corner sites on metal surfaces are considered to be the most active sites for carbon monoxide adsorption. This is due to the fact that metal atoms at these locations possess fewer neighbours than those at terraces/planes. Consequently, edge and corner sites possess a greater number of *d* electrons for π-bonding with adsorbed CO which in turn increases the π character and strength of the metal–carbon bond.

The presence of a tilted CO mode of adsorption may indicate a degree of support interaction incurred by reduction. This support interaction is manifested by partial encapsulation of the noble metal by the partially reduced CeO_2 support. Partial encapsulation increases the proximity of the noble metal and oxide support, hence, facilitating the coordination of both the C and O ends of the CO molecule. The role of Ce cations (acting as promoters) is associated with influencing the adsorption state of carbon monoxide by (a) enhancing the back-bonding through the metal, (b) an electrostatic effect, and/or (c) short-range chemical interactions (19). Noerskov *et al.* (51) and Van Santen (52) suggested that the promoter adsorbed on a metal surface creates a strong electrostatic field. In doing so, the promoter induces an increased population of the $2\pi^*$ CO orbital placed in the field created by the promoter. Additionally, the dipole of the adsorbed CO molecule may be changed as a result of the enhanced C–O intranuclear distance. The interaction of the oxygen end of the CO molecule with the support has been shown to favour dissociation of CO through lowering the activation energy by weakening of the strong C≡O bond (53).

Bands with similar behaviour were reported by Alekseev *et al.* (54) on the surface of (1.6%Rh–1.9%Nb)/SiO_2 reduced at 773 K and chemisorbed with 75 Torr of CO. Bands at 1704 and 1652 cm^{-1} were attributed to Rh–CO–Nb^{n+} complexes in different coordination environments. Binet *et al.* (30) suggested that bands at 1731 and 1628 cm^{-1}, produced on Pd/CeO_2 from the adsorption of CO, were due to tilted CO in the form of Pd_n–CO–Ce^{3+}, where *n* was 1 for the 1731-cm^{-1} band and 2 for the lower frequency band at 1628 cm^{-1}. Similarly, a band situated at 1660 cm^{-1} upon adsorption of CO on Rh/ZrO_2 was attributed to a bridged CO species bonded to Rh^0 particles through the C atom and also bonded to the coordinatively unsaturated Zr^{4+} ion via the O atom (55). Thus, by analogy to the above, the higher frequency band may be due a tilted CO species of the type Pt–CO–Ce^{3+} and the lower frequency band may be due a tilted CO species of the type Pt_2–CO–Ce^{3+}. Table 6 summarises the observed CO bands formed from ethanol as well as CO adsorption.

The Origin of the Band at 2112 cm^{-1}

It has been suggested that a band at 2118–2127 cm^{-1}, observed over evacuated CeO_2 at high temperatures, is attributed to electronic transition (a $2F_{5/2}$ to $2F_{7/2}$ transition) of Ce^{3+} cations (7). Although this may be plausible, our data do not agree with such an assignment for the following reasons: (1) CeO_2, both reduced and unreduced, shows the same band (Fig. 13). (2) Although the band at 2121 cm^{-1} did not increase upon CO adsorption and evacuation to 5×10^{-5} Torr, it did decrease with increasing temperature to a third of its level at ca. 673 K (Fig. 9). Such a decrease cannot reasonably be attributed to surface oxidation since CO is even a more powerful reducing agent than H_2. (3) TPD after CO adsorption over CeO_2 shows the desorption of CO_2, presumably resulting from CO oxidation (Fig. 7). (4) Ethanol-dosed Pt/CeO_2 surfaces show the same band at elevated temperatures when the bridged CO band disappears (Figs. 3 and 5). Thus, our data suggest that this band is attributed to CO adsorbed on defected surfaces of CeO_2 such as Ce^{3+} cations.

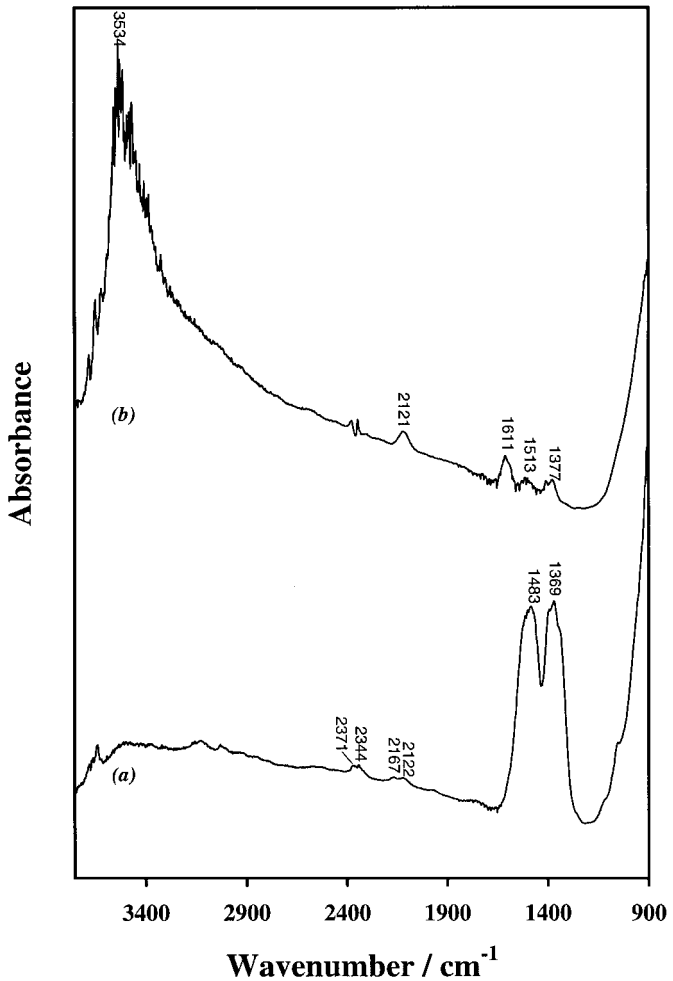

FIG. 13. IR spectra of blank undosed (a) unreduced and (b) H_2-flow reduced CeO_2 surfaces.

C. Acetaldehyde Formation

Evidence of acetaldehyde formation was given by its desorption during TPD (Figs. 1 and 4) and steady state reaction as well as by IR (Figs. 2, 3, and 5). Previous work on CeO_2 alone has shown only traces of the formation of acetaldehyde during ethanol TPD, while IR of ethanol has shown no evidence of adsorbed acetaldehyde species at all (13). Thus, Pt considerably enhances the dehydrogenation route. This enhancement is most likely due to blocking of the direct oxidation route to acetates due to partial reduction of the support in addition to accelerating the β-hydrogen elimination as follows:

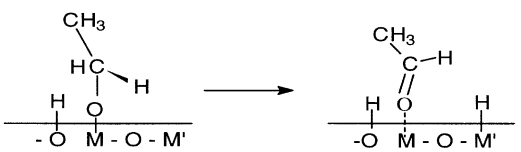

IR: 1700 cm^{-1}, T_P (TPD): 465-665 K [3]

where M is Ce, M' is Ce or Pt, and T_p is the peak desorption temperature.

D. Crotonaldehyde and Benzene Formation

Evidence of adsorbed crotonaldehyde species has been given by IR (Figs. 3 and 5). Crotonaldehyde is the result of β-aldolisation of acetaldehyde on the surface of CeO_2. The absence of crotonaldehyde over CeO_2 alone (from ethanol) is in fact due to the absence of acetaldehyde formation. Previous work showed the formation of crotonaldehyde from acetaldehyde over CeO_2 by TPD as well as IR (14). Crotonaldehyde was also observed, from acetaldehyde, over other surfaces such as TiO_2 (15), Al_2O_3 (16), and UO_3 (16), (the reaction mechanism was presented and discussed in other works (15)). Its formation requires, besides Lewis acid sites at which to bind two molecules of acetaldehyde, a base site to abstract a hydrogen atom from the α-position of the carbonyl. However, the amount of crotonaldehyde desorbed during TPD is extremely small over the unreduced catalysts and no detectable desorption was observed over the reduced one. This latter result can be explained as follows. Once crotonaldehyde is formed, it can react with another adsorbed acetaldehyde (via the same β-aldolisation reaction) giving 2,4-hexadienal as follows.

$$CH_3CH{=}CHCHO_{(ads)} + CH_3CHO_{(ads)} \rightarrow CH_3CH{=}CH{-}CH{=}CH{-}CHO_{(ads)} + H_2O. \quad [4]$$

This bulky molecule diffusing slowly in the pores will be subject to further attack by active sites of the catalyst: in other words, in contact with Pt it may suffer a C–H bond dissociation of the methyl group which after intramolecular cyclisation followed by H_2O elimination may give benzene with the simultaneous oxidation of partially reduced Ce cations as shown in Scheme 1. Indeed, considerable amounts of benzene are observed during TPD.

CONCLUSION

The reaction of ethanol over both unreduced and H_2-reduced Pt/CeO_2 proceeds via an ethoxide intermediate. Acetaldehyde, formed by the oxidative dehydrogenation of these ethoxide species, was observed to undergo β-aldolisation to form adsorbed crotonaldehyde species. TPD studies have shown that, in addition to unreacted ethanol and other reaction products, benzene is desorbed

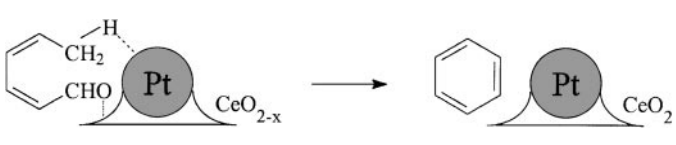

SCHEME 1. Schematic of proposed mechanism for benzene formation over Pt/CeO_2; 2,4-hexadienal is formed as shown in Eq. [4].

in appreciable amounts. The formation of benzene most likely occurs through further reaction of adsorbed crotonaldehyde with another acetaldehyde species in the vicinity of Pt clusters.

A rationalisation for the types of adsorbed ethoxide species on the Pt/CeO_2 surface has been discussed in terms of surface morphology of CeO_2 as well as surface defects introduced due to Pt clusters. Several modes of adsorbed CO have been observed; these include linear, bridged, and tilted. In particular, the presence of tilted CO species indicates the involvement of metal–support interactions. In addition, carbonite dianion species have also been detected following the adsorption of CO on the surface of H_2-reduced Pt/CeO_2. Overall, in the reaction of ethanol, Pt/CeO_2 behaves similarly to Pd/CeO_2 (13), although with considerably greater formation of benzene.

REFERENCES

1. Yao, H. C., and Yao, Y. F., *J. Catal.* **86**, 254 (1984).
2. Murrel, L. L., Tauster, S. J., and Anderson, D. R., *Stud. Surf. Sci. Catal.* **71**, 275 (1991).
3. Trovarelli, A., Dolcetti, G., de Leitenburg, C., and Kaspar, J., *Stud. Surf. Sci. Catal.* **75**, 2781 (1993).
4. Morrison, S. J., M.Sc. thesis, The University of Auckland, New Zealand, 1998.
5. Li, C., Domen, K., Maruya, K., and Onishi, T., *J. Catal.* **125**, 445 (1990).
6. Lamotte, J., Moravek, V., Bensitel, M. and Lavalley, J. C., *React. Kinet. Catal. Lett.* **36**, 113 (1988).
7. Binet, C., Badri, A., and Lavalley, J. C., *J. Phys. Chem.* **98**, 6392 (1994).
8. Bensitel, M., Moravek, V., Lamotte, J., Saur, O., and Lavalley, J. C., *Spectrochim. Acta* **43**, 1487 (1987).
9. Greenler, R.G., *J. Chem. Phys.* **37**, 2094 (1962).
10. Kondo, J., Sakata, Y., Maruya, K., Tamaru, K., and Onishi, T., *Appl. Surf. Sci.* **28**, 475 (1987).
11. Demri, D., Chateau, L., Hindermann, J. P., Kiennemann, A., and Bettahar, M. M., *Mol. Catal. A: Chem.* **104**, 237 (1996).
12. Badri, A., Binet, C., and Lavalley, J. C., *J. Chem. Soc. Faraday Trans.* **93**, 1159 (1997).
13. Yee, A., Morrison, S. J., and Idriss, H., *J. Catal.* **186**, 279 (1999).
14. Idriss, H., Diagne, C., Hindermann, J. P., Kiennemann, A., and Barteau, M. A., *J. Catal.* **155**, 219 (1955).
15. Idriss, H., Kim, K. S., and Barteau, M. A., *J. Catal.* **139**, 119 (1993).
16. Madhavaram, H., and Idriss, H., submitted for publication.
17. Davis, J. L., and Barteau, M. A., *Surf. Sci.* **235**, 235 (1993).
18. Shekhar, R., Barteau, M. A., Plank, R. V., and Vohs, J. M., *J. Phys. Chem.* **101**, 7939 (1997).
19. Boujana, S., Demri, D., Cressely, J., Kiennemann, A., and Hindermann, J. P., *Catal. Lett.* **7**, 359 (1990).
20. Madhavaram, H., and Idriss, H., *Stud. Surf. Sci. Catal.* **110**, 265 (1997).
21. Idriss, H., Libby, M., and Barteau, M. A., *Catal. Lett.* **15**, 13 (1992).
22. Blyholder, G., *J. Phys. Chem.* **68**, 2772 (1964).
23. Binet, C., Badri, A., Boutonnet-Kizling, M., and Lavalley, J. C., *J. Chem. Soc. Faraday Trans.* **90**, 1023 (1994).
24. Li, C., Sakata, Y., Arai, T., Domen, K., Maruya, K., and Onishi, T., *J. Chem. Soc. Faraday Trans. 1* **85**, 1451 (1989).
25. Li, C., Sakata, Y., Arai, T., Domen, K., Maruya, K., and Onishi, T., *J. Chem. Soc. Faraday Trans. 1* **85**, 929 (1989).
26. Bozon-Verduraz, F., and Bensalem, A., *J. Chem. Soc. Faraday Trans.* **90**, 653 (1994).
27. Jin, T., Zhou, Y., Mains, G. J., and White, J. M., *J. Phys. Chem.* **91**, 5931 (1987).
28. Hadjiivanov, K. I., *J. Chem. Soc. Faraday Trans.* **94**, 1901 (1998).
29. Bensalem, A., Muller, J. C., Tessier, D., and Bozon-Verduraz, F., *J. Chem. Soc. Faraday Trans.* **92**, 3233 (1996).
30. Binet, C., Jadi, A., Lavalley, J. C., and Boutonnet-Kizling, M., *J. Chem. Soc. Faraday Trans.* **88**, 2079 (1992).
31. Badri, A., Binet, C., and Lavalley, J. C., *J. Chem. Soc. Faraday Trans.* **92**, 1603 (1996).
32. Sheu, L. L., and Sachtler, W. M. H., *J. Mol. Catal.* **81**, 267 (1993).
33. Brunauer, S., Emmet, P. H., and Teller, E., *J. Am. Chem. Soc.* **60**, 309 (1938).
34. Millar, G. J., Newton, D., Bowmaker, G. A., and Cooney, R. P., *Appl. Spectrosc.* **48**, 827 (1994).
35. Ko, E. I., Benziger, J. B., and Madix, R. J., *J. Catal.* **62**, 264 (1990).
36. Busca, G., and Lorenzelli, V., *Mater. Chem.* 89 (1982).
37. Baird, R. J., Ku, R. C., and Wynblatt, P., *Surf. Sci.* **97**, 346 (1980).
38. Root, T. W., Schmidt, L. D., and Fisher, G. B., *Surf. Sci.* **150**, 173 (1985).
39. Diaz, A. L., Quigley, W. W. C., Yamamoto, H. D., and Bussell, M. E., *Langmuir* **10**, 1461 (1994).
40. Diagne, C., Idriss, H., Pepin, I., Hindermann, J. P., and Kiennemann, A., *Appl. Catal.* **50**, 43 (1989).
41. Hayden, B. E., and Bradshaw, A. M., *Surf. Sci.* **125**, 787 (1987).
42. Persson, B. N. J., Tushaus, M., and Bradshaw, A. M., *J. Chem. Phys.* **92**, 5034 (1990).
43. Chang, S. C., and Weaver, M. J., *J. Phys. Chem.* **95**, 5391 (1991).
44. De la Cruz, C., and Sheppard, N., *Spectrochim. Acta* **50**, 271 (1994).
45. Sanderson, R. T., "Chemical Bonds and Bond Energy," 2nd ed., Academic Press, New York, 1976.
46. Lee, W. T., Thomas, F., and Masel, R. I., *Surf. Sci.* **418**, 479 (1998).
47. Sexton, B. A., *Surf. Sci.* **102**, 271 (1981).
48. Sayle, T. X. T., Parker, S. C., and Catlow, C. R. A., *Surf. Sci.* **316**, 329 (1994).
49. Norenberg, H., and Briggs, G. A. D., *Surf. Sci.* **402**, 734 (1998).
50. Sayle, T. X. T., Parker, S. C., and Catlow, C. R. A., *J. Phys. Chem.* **98**, 13625 (1994).
51. Noerskov, J. K., Holloway, S., and Lang, N. D., *Surf. Sci.* **137**, 65 (1984).
52. Van Santen, R. A., *in* "Proceedings, 8th International Congress on Catalysis, Berlin, 1984," Vol. 4, p. 97. Dechema, Frankfurt-am-Main, 1984.
53. Ichikawa, M., Fukushima, T., and Shikakura, K., *in* "Proceedings, 8th International Congress on Catalysis, Berlin, 1984," Vol. 2, p. 69. Dechema, Frankfurt-am-Main, 1984.
54. Alekseev, O. S., Beutel, T., Paukshtis, E. A., Ryndin, Y. A., Liknolobov, V. A., and Knozinger, H., *J. Mol. Catal.* **92**, 217 (1994).
55. Guglielminotti, E., *J. Catal.* **120**, 287 (1989).
56. Kim, M., Sim, W. S., and King, D. A., *J. Chem. Soc. Faraday Trans.* **92**, 4781 (1996).
57. Mitchell, W. J., Xie, J., Jachimowski, T. A., and Weinberg, W. H., *J. Am. Chem. Soc.* **117**, 2606 (1995).
58. Underwood, R. P., and Bell, A. T., *J. Catal.* **111**, 325 (1988).